BULETINUL INSTITUTULUI POLITEHNIC DIN IAŞI
Publicat de
Universitatea Tehnică „Gheorghe Asachi” din Iaşi
Volumul 67 (71), Numărul 1, 2021
Secţia
CHIMIE şi INGINERIE CHIMICĂ

EFFECT OF METAL SYNERGY AND LOADING ON BINARY W-Mo/HZSM-5 CATALYST FOR NON-OXIDATIVE CONVERSION OF METHANE INTO CARBON AND PETROCHEMICALS

BY

RONALD MUSAMALI* and YUSUF ISA

Durban University of Technology,
Chemical Engineering department, South Africa

Received: February 2, 2021
Accepted for publication: March 10, 2021

Abstract. Processing of energy from fossil fuels is associated with emission of carbonaceous compounds. Therefore, non-oxidative conversion of methane into carbon and petrochemicals remediates emission of these greenhouse gases into the atmosphere. This present study demonstrates the development of stable, durable, and tunable binary catalyst systems comprising of W, &Mo supported on HZSM-5. The catalyst systems were synthesized by incipient wetness impregnation, characterized, and tested for non-oxidative methane conversion in a packed bed reactor. Reactor effluents were analyzed using gas chromatography. Based on the results obtained, competing reactions between different metal species, loading, and synergism influenced product distribution. Carburized molybdenum (Mo_2C) on HZSM-5 zeolite alone exhibited low catalytic activity but on promotion with W, its activity increased tremendously. The reaction entailed dissociation of methane molecules on carburized Mo to form C_2-species as primary intermediates which were further oligomerized into aromatics and higher hydrocarbons in the channels of HZSM-5 zeolite.

Keywords: Methane; non-oxidative; petrochemical; W-Mo/HZSM-5 catalyst.

*Corresponding author; *e-mail*: musamalironald@gmail.com

1. Introduction

Major energy sources are of fossil origin (Chen *et al*., 2018). Other sources of energy include hydro, wind, solar, geothermal, tidal and biomass. Mature energy producing technologies using fossil fuels as primary energy sources are associated with emission of greenhouse gases which are harmful to the environment (Brandt *et al*., 2018). Notable greenhouse gases are water vapour, carbon dioxide, methane, nitrous oxide, ozone, chlorofluorocarbons and hydrofluorocarbons. Non-oxidative conversion of methane into fuels and chemicals can be envisaged as a remedy in reducing this greenhouse gas emissions into the atmosphere. Apart from pollution, these major energy producing technologies are faced will various challenges such as high initial capital investment on equipment, process scale-up and thermodynamic challenges which affect their development to commercial scale (Wassie *et al*., 2018). Therefore, there is need to explore other methods of producing clean energy.

Non-oxidative conversion of methane (NOCM) is one such option. It is a complex reaction mechanism which occurs stepwise (Karakaya *et al*., 2018). According to (Varghese *et al*., 2018), a methane molecule first dissociates on the metal to form M-CxHy, and then proceed to form ethane and ethylene before reacting with metallic oxide to form metallic carbide. The formed carbide is either converted into benzene or the carbonaceous species is reacted with M-H to form benzene. When a transition metal catalyst has been used, the methane molecule is activated on the precious metal to form metal carbide and hydrogen and then the carbide is hydrogenated by into higher hydrocarbons.

Non-oxidative conversion of methane occurs via different pathways depending on the catalyst used and the reaction conditions. Remarkable catalyst activity takes place at > 800°C. According to (Karakaya and Kee, 2016), non-oxidative conversion of methane takes place according the following globally recognised reactions.

$$2CH_4 \rightarrow C_2H_6 + H_2 \quad (1)$$

$$2CH_4 \rightarrow C_2H_4 + 2H_2 \quad (2)$$

$$6CH_4 \rightarrow C_6H_6 + 9H_2 \quad (3)$$

$$CH_4 \rightarrow C + 2H_2 \quad (4)$$

Major products of non-oxidative conversion of methane are carbon and petrochemicals. Ethylene and propylene are important sources of plastic products and rubber. Aromatics like benzene, toluene and xylenes (BTX) find a lot of application in chemical industry. Benzene is a raw material for making dyes and synthetic detergents, and benzene and toluene are used for making polyurethanes. Most manufacturers use xylenes to manufacture plastics and synthetic fibers. A typical NOCM reaction has low conversion and limited selectivity to desired products (Liu *et al*., 1999). For almost a decade from now,

NOCM reaction has been studied by several research groups; (Xu *et al*., 1994; Solymosi *et al*., 1996), and (Wang *et al*., 1997) using Mo/HZSM-5 catalyst. From their studies, they concluded that the acidity of HZSM-5 and carburized molybdenum combined to form an active species for hydro condensation of methane towards benzene on Mo/HZSM-5 catalysts. Further, (Wang *et al*., 1996) and (Ohnishi *et al*., 1999) demonstrated that methane is dehydrocondensed into various aromatics and naphthalene on Mo/HZSM-5 and Mo/HZSM-5 doped with iron and cobalt. Carburized Mo activates the methane C-H bonds and form the first C-C intermediate species (Abdelsayed *et al*., 2015). These C_2 intermediates oligomerizes on the acid sites in HZSM-5 to form aromatic products (Xu and Lin, 1999). The similarity between HZSM-5 pores and the dynamic pore diameter of benzene (Ma *et al*., 2013) favors its high shape selectivity. Catalyst deactivation due to cocking by deposited carbon has been a major bottleneck to commercialization of this process. To address this coking problem, a lot of research work has been expended in this area to suppress coke formation and improve selectivity towards aromatics. Such efforts have concentrated on enhancement of the zeolite surface area (Ding *et al*., 2002), promotion with noble metals (Burns *et al*., 2006) , periodic CH_4/H_2) switching (Rodrigues and Monteiro, 2008) increasing the number and density of acid sites on HZSM-5 and tilting the reaction equilibrium by removing hydrogen from the reaction using membrane reactors (Liu *et al*., 2002).

Zeolites have been used extensively as catalyst supports in many industrial reactions such as hexane cracking, disproportionation of toluene, alkylation of benzene, xylene isomerization and conversion of methyl chloride to ethylene due to their heat stability (Ali *et al*., 2002) and enhanced surface area (Fujikawa *et al*., 2000). Structural and acidic properties of HZSM-5 zeolite enhances the valence location of the noble metal. As reported elsewhere (Khan *et al*., 2018), catalytic activity of common acidic supports in methane conversion have been found to occur according to the following order; HZSM-5 > γ-Al_2O_3 > SiO_2 MgO > ZrO_2 with benzene forming only on HZSM-5 and γ-Al_2O_3.

Promotion of Mo/HZSM-5 with Zn (Xu *et al*., 2011) and W (Zeng *et al*., 1998) improved its stability and selectivity towards benzene at 1073K. In contrast, Xu (Xu *et al*., 2012) did not report any positive improvement on catalyst stability on Mo/HZSM-5 was promoted with Zn. Very little data has been reported on double promotion of HZSM-5 catalyst for methane aromatization (Sily *et al*., 2006) perhaps due to its complexity. The necessity to utilize methane gas as a source of raw material for fuels and industrial chemicals is of great interest to present day researchers. Therefore, there is need to develop an efficient process for non-oxidative conversion of methane to realize high selectivity towards these petrochemicals. To the best of our knowledge, no work been work has been done in synthesizing catalyst systems to quantitatively control methane conversion and product distribution in non-oxidative methane conversion.

Therefore, this present work investigates the synergetic effect of noble metals in a binary W-Mo/HZSM-5 catalyst systems in non-oxidative conversion of methane into carbon and other value-added chemicals. Such an invention is aimed at developing a stable, active and durable catalyst systems for quantitative control of product distribution in methane conversion to carbon and petrochemicals.

2. Experimental

2.1. Materials and Methods

Chemicals for catalyst precursors were purchased and used as they were. Catalyst precursors were; Ammonium ZSM-5 (NH_4ZSM-5 SiO_2/Al_2O_3 = 50) 99.8% pure from Zeolyst International-USA, Activated carbon 99.9% pure from Merck-USA, Ammonium heptamolybdate $(NH_4)_6Mo_7O_{24}{\cdot}4H_2O$ 99.8% pure from Merck-USA, Ammonium Para tungstate ATP) $(NH_4)_{10}W_{12}{\cdot}4H_2O$ 99.9% from Merck-USA, hydrogen gas (99% pure from Afrox-South Africa), methane feed mixture (50%CH_4:50%Ar from Afrox-South Africa), nitrogen gas (99% pure from Afrox-South Africa) and distilled water. The prepared catalyst materials were designated according to %wt as shown in Table 1 below.

Table 1
Designation of Various Binary Catalysts According to Composition

No.	Catalyst	Composition
1.	4.8M/HZSM-5	4.8%Mo – 95.2%HZSM -5
2.	4.8W/HZSM-5	4.8%W – 95.2%HZSM-5
3.	2.4W2.4M/HZSM-5	2.4%W – 2.4%Mo – 95.2%HZSM -5
4.	1.8W3.0M/HZSM-5	1.8%W – 3.0%Mo – 95.2%HZSM -5
5.	3.0W1.8M/HZSM-5	3.0%W – 1.8%Mo – 95.2%HZSM -5

The catalysts in Table 1 above were synthesized by incipient wetness impregnation, dried, and calcined before characterization and subsequent application on NOCM reaction.

2.2. Catalyst Characterization

Crystallinity of synthesized catalysts was done using X-ray diffraction (XRD) equipment, BRUKER AXS (Germany) equipped with diffractometer-D8 Advance**.** The measurements were done using a continuous J-J scan in locked coupled mode at Cu-Ka radiation (lKa_1=1.5406Å).

Porosity, surface area, and particle size distribution of the synthesized catalysts were determined from N_2 adsorption data at -196°C by use of Brunauer-Emmet Teller (BET) equipment, Micromeritics Tristar II 3020. Structural properties of the freshly synthesized catalysts were done using a

Scanning electron microscopy (SEM) equipment (FEI Nova Nano SEM 230) equipped with field emission gun that was used to analyse composition of alloy catalysts. The samples were imaged using the high-resolution immersion lens. The EDS detector used was an Oxford X-Max, using INCA software (Landing E 5.00KeV, working distance HFW 5.97-29.8, Sopt3.5 and WD (5.8-6.7). Image-J software was used to determine the particle size and distribution of crystallites.

IR measurements were done in pyridine adsorption. Each powder of the 4.8 %wt metal loading on HZSM-5 (SiO_2/Al_2O_3=50) was pressed into a self-supporting wafer (2.0 mm ID,15-18 mg/cm^2) with a pressure of 500 kgf/cm^2. The wafer was placed in an IR cell equipped with CaF_2 window. The IR spectra were recorded using a step-scan Fourier transform infrared spectrometer (BIO-RAD FTS-60A/896) with a resolution of 4 cm^{-1}, and a co-accumulation of 64 interferograms to improve sign to noise ratios of the IR spectra. The IR measurement was conducted by exposure of the disk of HZSM-5 after evacuating at 723K for 2 h to the pyridine vapor of 1.2 kPa at 300K.

Transmission Electron Microscopy (TEM) analysis was used to obtain information on particle size, shape and morphology of deposited carbon nanomaterial on the catalyst. The equipment used in the analysis was (JEOL JEM-1010-South Korea, equipped with a high-resolution camera). Imaging of test samples were done at different magnification levels to obtain fine details of carbon nanomaterial.

2.3. Catalyst Evaluation

Non-oxidative methane conversion experiments were performed in a packed bed reactor of dimensions (ID 8.6 mm, OD 12.6 mm and L-545 mm) at 750℃ , GHSV 0.96 Lg^{-1}cat.h^{-1}, and at 1 atm for 4 h time on stream. The reactor was first stuffed with Quartz wool at the middle to hold the catalyst, loaded with 0.4 g of the catalyst and then purged with nitrogen gas at a flow rate of (100 mL/min) at 400℃ for 30 min to remove residual moisture and volatile matter. Heating was programmed at $5\,℃/min$ up to the desired reaction temperature. Then methane gas mixture (50%CH_4:50%Argon) was introduced into the reactor at different GHSVs. The outlet of the reactor was connected to a condenser and then to a conical volumetric flask to collect the pyrolysis gas. Both liquid and gaseous products from the reaction were analyzed using a gas chromatograph. Mass balance based on total gas flow rate in and out of the reactor was calculated using Eq. (5) below since the mass flow rate of argon as the internal standard gas remains the same in and out of the reactor. Methane% conversion and selectivity of each product containing carbon atom on carbon basis (S^{carbon}) can be calculated from Eq. (6) and Eq. (7), respectively. Coke selectivity was calculated from (100%-sum of product % selectivities).

In Eqs. (5) - (7), *F*, *X* and N^{carbon} represent the total gas flow rate, mole fraction, and carbon number in the hydrocarbon molecule, respectively. For each NOMC run, time on stream was 4 h. Catalytic activity of each catalyst was evaluated in terms of methane conversion, and selectivity towards C_2 hydrocarbons, benzene, toluene, xylene, and coke.

The amount of methane consumed can be calculated from Eq. (5) below.

$$F^{inlet} \times X_{CH4}inlet - F^{outlet} \times X_{CH4}outlet = \text{Methane reacted} \quad (5)$$

Methane conversion and selectivity towards C_2 hydrocarbons, benzene, toluene, xylene, hydrogen and coke were determined by applying the equations below.

$$\text{Conversion (\%)} = \frac{F^{inlet} \times X_{CH4inlet} - F^{outlet} \times X_{CH4outlet}}{F^{inlet} \times X_{CH4inlet}} \text{ x } 100 \quad (6)$$

$$\text{Selectivity Hydrocarbon (\%)} = \frac{F^{outlet} \times X_{CxHy} \times N_{carbon}}{F^{inlet} \times X_{CH4in} - F^{outlet} \times X_{CH4\,out}} \text{ x } 100 \quad (7)$$

Where *N* is the carbon number in the hydrocarbon which represent the stoichiometric ratio.

$$\text{Coke selectivity (\%)} = 100\% - \sum Pi\% \quad (8)$$

Where $\sum Pi$, is the sum of product selectivity (%), other than coke; Coke selectivity (%) was calculated from Eq. (8) above.

2.4. Results and Discussion

2.4.1. *Catalyst Characterization*

Synthesized catalysts were characterized for crystallinity, surface area, structural properties, and acidity using XRD, B.E.T, SEM, and FT-IR techniques, respectively.

2.4.1.1. *XRD-Analysis*

XRD patterns of HZSM-5 zeolite and other catalyst systems shown in Fig. 1 below confirm the presence of distinct HZSM-5, and target metal oxide phases. In all the five catalysts, sharp peaks at 2θ=8.0°, 8.9°, 9.1°, 14.9°, 20.9° and 23.2° are assigned to HZSM-5 according to diffraction peaks classification in JCPDS File no. (00-044-002). These magnificent peaks tend to mask the peaks of noble metals in each catalyst due low metal loading

(4.8%metal/HZSM-5). In catalyst 4.8M/HZSM-5, peaks at 2θ = 34.3°, and 49.2° are assigned to MoO_3 corresponding to those in JCPDS File no. (05-0508). In catalyst 4.8W/HZSM-5, peaks at 2θ=23.2°, 29.0°, 42.1°, and 50.4° are assigned to orthorhombic WO_3 according to diffraction peaks classification in JCPDS File no. (32-1394). Upon equal metal loading in catalyst 2.4W2.4M/HZSM-5, peaks corresponding to WO_3 and MoO_3 become very faint due to low metal loading in the catalyst. In all catalysts, corresponding metal oxides from their precursors are clearly formed after calcination. Less sharpness of metal oxide peaks can also be attributed to their high dispersion in the catalyst. After impregnating the zeolite with the oxides of WO_3 and MoO_3, peak intensity decreased but the peak positions remained unchanged. This implies that, impregnating the zeolite with metal oxides did not alter the zeolite structure. This observation is in consistent with what was reported elsewhere (Bajec *et al.*, 2019).

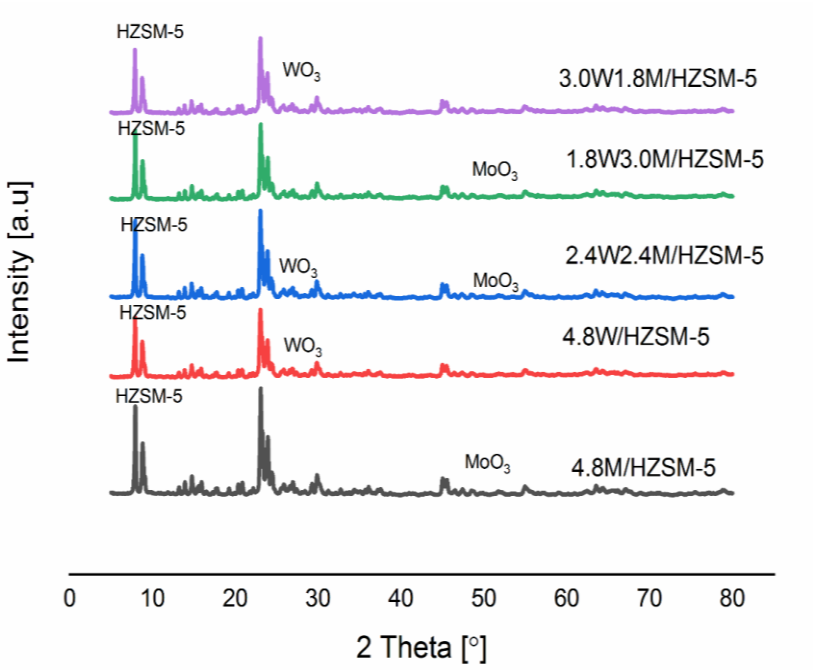

Fig. 1 – XRD patterns for catalyst 4.8M/HZSM-5, 4.8W/HZSM-5, 2.4W2.4M/HZSM-5, 1.8W3.0M/HZSM-5, and 3.0W1.8M/HZSM-5.

2.4.1.2. *SEM Analysis*

Scanning electron microscopy was used to obtain information on catalyst crystallite size, shape and morphology. Image-J software use used to obtain information on crystallite size. In Fig. 2 below, catalyst 4.8M/HZSM-5

shows clearly defined structures of nano particles which assume the shape of tri lobes, Quadra lobes and spheres. The crystallite size ranged from 2.57-23.52 nm with an average crystallite size of 5.63 nm. The neatness of stacked structures on top of each other is an indication of little agglomeration after calcination. Similar structures also manifest in catalyst 4.8W/HZSM-5 with the crystallite size ranging from 2.57-18.82 nm. Small values of "maximum crystallite" size implies less agglomeration and clumping of catalyst crystallites. Neat crystallite structures with cornflake-like shapes and tri lobes manifest themselves in this catalyst. When metal loading was equal in catalyst 2.4W2.4M/HZSM-5, we saw well-defined tetrahedral and cubic structures of nanoparticles with crystallite size ranging from 2.57-23.76 nm. In catalyst 1.8W3.0M/HZSM-5, crystallite sizes ranged from 2.57-16.94 nm. Large irregular and cube shaped structures are seen in catalyst 3.0W1.8M/HZSM-5 with particle sizes ranging from 2.57 to 29.42 nm. Big lumps of catalyst crystallites are seen clumped together due to agglomeration after calcination. In a nutshell, all the four catalyst crystallite sizes ranged from 2.57 to 29.42 nm, which is an indication that all the catalyst crystallites were nanomaterials.

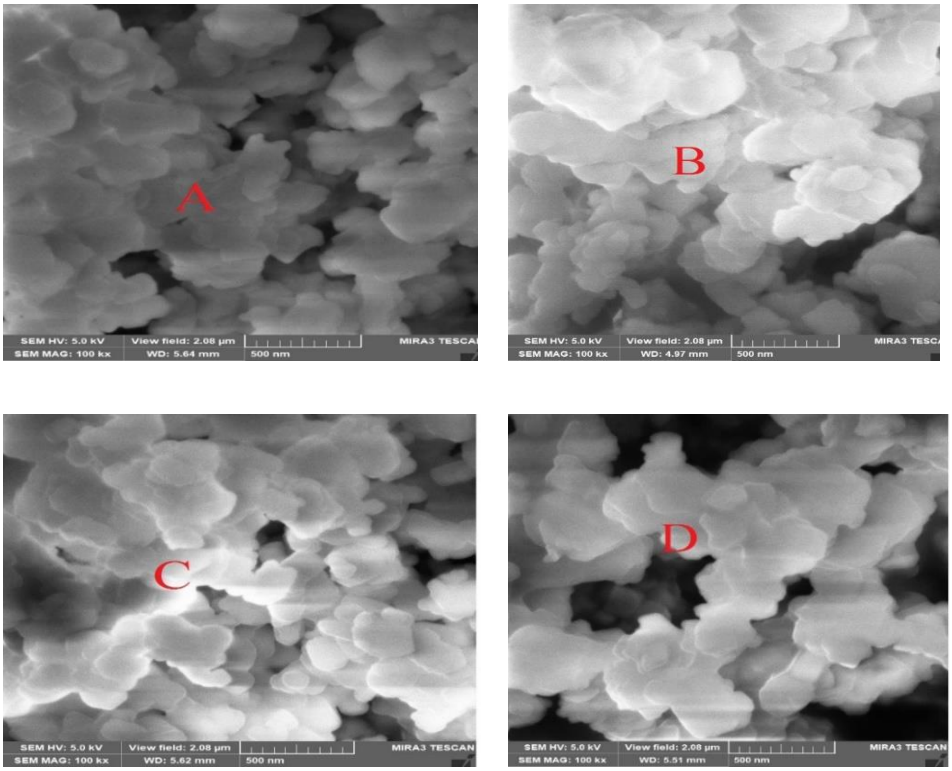

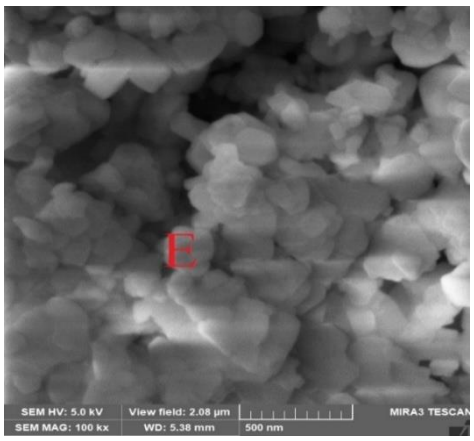

Fig. 2 – SEM Image of catalysts; A(4.8M/HZSM-5), B(4.8W/HZSM-5), C(2.4W2.4M/HZSM-5), D(1.8W3.0M/HZSM-5), and E(3.0W1.8M/HZSM-5).

2.4.1.3. *BET Analysis*

From BET analysis results in Table 2 below, we can see that all the catalysts had a surface area above 240 m^2g^{-1}. The reference HZSM-5 zeolite had the following structural properties; surface area 496 cm^2g^{-1}, pore volume 0.1787 m^3g^{-1} and pore size of 24.748 Å.

Impregnating the zeolite with oxides of tungsten and molybdenum greatly altered its surface properties. After loading HZSM-5zeolite with 4.8% Mo, we observed a reduction in surface area, pore volume and pore size by 43.35%, 35.59%, and 10.51% respectively. In catalyst 4.8W/HZSM-5, we observed a tremendous decrease in surface area and pore volume in reference to the parent zeolite but with a huge increase in pore size. A further reduction in surface area and pore volume was seen in catalyst 2.4W2.4M/HZSM-5 even though, a notable increase in pore size was recorded in reference to the parent zeolite. Reducing the quantity of W and increasing the amount of Mo in the overall 4.8% metal/support catalyst system led to an increase in surface area, pore volume and pore size. On the other hand, increasing the quantity of W and reducing the amount of Mo in the overall 4.8% metal/support catalyst system only increased the catalyst surface area and pore size.

From the above trend, we see that the refence HZSM-5 zeolite is a high surface area mesoporous material. Impregnating the zeolite with the oxides of WO_3 and MoO_3 reduces its surface area and pore volume. Interestingly, when the amount of W is higher than Mo in the overall 4.8% metal/support catalyst system, there was an increase in surface area and pore size. In catalyst 3.0W1.8M/HZSM-5, pore size increased by 17.33% in reference to the parent zeolite. We therefore believe that molybdenum easily entered the zeolite

structure thereby altering its structural properties whereas tungsten was responsible for the generation of more mesopores in the zeolite structure.

Table 2
Catalyst Surface Area, Pore Volume, and Pore Size

No.	Catalyst	BET Surface area (cm^2/g)	Pore volume (cm^3/g)	Pore size (Å)
1.	HZSM-5	496	0.178	24.749
2.	4.8M/HZSM-5	281	0.115	22.148
3.	4.8W/HZSM-5	311	0.118	29.178
4.	2.4W2.4M/HZSM-5	243	0.127	27.014
5.	1.8W3.0M/HZSM-5	287	0.166	25.638
6.	3.0W1.8M/HZSM-5	301	0.097	29.936

2.4.1.4. *FT-IR Analysis*

According to the analysis of attribution by Frixione-Kunszt-Signer (FKS) method (Cheng *et al.*, 2017), the absorption peaks at 1226 cm^{-1}, 1100 cm^{-1}, 796 cm^{-1}, 624 cm^{-1}, 547 cm^{-1} and 453 cm^{-1} were ascribed to the characteristic framework vibration peaks of HZSM-5 zeolite *i.e.* the symmetric stretching vibration, anti-symmetric stretching vibration, vibration of five membered ring and block structure, and of T-O bending vibration peaks, respectively. The anti-symmetric stretching vibration peak at 1226 cm^{-1} is very sensitive to Si/Al ratio of HZSM-5, with the removal of aluminum species in the skeleton changing the vibration to higher frequencies (Cheng *et al.*, 2017). From literature, Mo oxide species associated with Bronsted acid sites are responsible for no-oxidative aromatization of methane leading a reduction in the intensity of Bronsted acid sites (Liu *et al.*, 2011). Enhanced Bronsted acidity is responsible for higher dispersion of metal oxides in the zeolite and improves the interaction between the metal oxides and zeolite thereby improving catalyst stability (Liu *et al.*, 2004).

From the FT-IR spectra in Fig. 3 below, the catalyst lattice vibrations were recorded between 500-4000 cm^{-1}. From the figure, we see notable peaks in the figure print region, especially at 1071-1080 cm^{-1}, and 542-545 cm^{-1}. Bands between 1071-1080 cm^{-1} are assigned to asymmetric stretching, bands at 542-545 cm^{-1} represent double ring while bands at 429-545 cm^{-1} represent T-O bending vibration of internal tetrahedral T=Si or T=Al. From literature (Tan *et al.*, 2002), these absorption bands at 1080 cm^{-1}, 810 cm^{-1} and 560 cm^{-1} are associated with internal linkages in SiO_4 (or AlO_4) tetrahedral and are very responsive to structural changes. The characteristic bands at 548 cm^{-1} and 1226 cm^{-1} are associated with ZSM-5 (Tan *et al.*, 2002). The peak positions in the spectra suggest a little shift in the peak position in the frequency of 548 cm^{-1} or 1226 cm^{-1} adsorption band which can be attributed to dealumination of the of

the zeolite lattice (Campbell *et al.*, 1996) after calcination. From literature, surface and structural properties of HZSM-5 greatly influence the interaction Mo species with the HZSM-5 zeolite. As reported elsewhere, pure HZSM-5 zeolite comprises of three hydroxyl groups, Bronsted acidity (≡Al-OH-Si≡), silanol groups (Si-OH), and extra framework aluminium (Al-OH). Since the densities of these functional groups are different, their interactions with the zeolite are different too. Therefore, the composition of Si/Al ratio of the zeolite greatly influences the interaction of the surface molybdate and the support.

Impregnation of the zeolite with WO_3 and MoO_3 reduces the intensity of acid sites on the external surface of HZSM-5 zeolite and the number of molybdenum species deposited on the external surface during the ion exchange process (Wu *et al.*, 2005). Since the characteristic vibration peaks of HZSM-5 remained nearly unchanged, we can conclude that impregnation of HZSM-5 with WO_3 and MoO_3 only shifted the peaks from 1071 cm^{-1} to 1080 cm^{-1} but did not alter the basic framework of HZSM-5 zeolite.

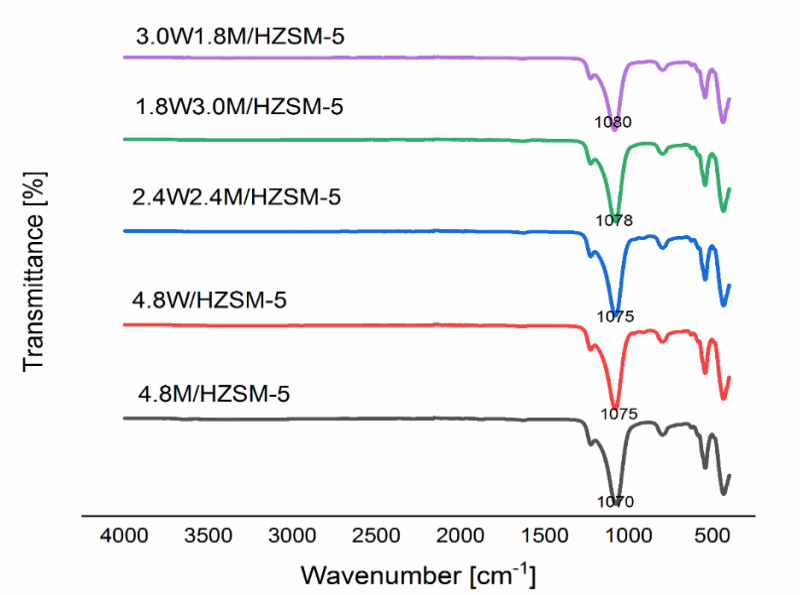

Fig. 3 – FT-IR spectra of catalysts 4.8M/HZSM-5, 4.8W/HZSM-5, 2.4W2.4M/HZSM-5, 1.8W3.0M/HZSM-5, and 3.0W1.8M/HZSM-5.

2.4.2. *Catalyst Evaluation*

Methane reaction studies were conducted in a packed bed reactor at 750℃ , GHSV 0.96 $Lg^{-1}cat.h^{-1}$, and at 1 atm for 4 h time on stream to study the effect of metal synergy on methane conversion and product distribution. From Table 3 below, catalyst 4.8M/HZSM-5 was least active in methane conversion

and highly selective towards toluene while catalyst 4.8W/HZSM-5 was most active in methane conversion, most selective towards coke but with moderate selectivity towards benzene. However, when the two metals W, and Mo were loaded on HZSM-5 in equal quantities, we saw a reduction in methane conversion, good selectivity towards benzene and an increase in both C_2 and least selectivity towards coke. From the results obtained, it can be inferred that Mo on HZSM-5 was less active in methane conversion but most selective towards C_2 hydrocarbons. Therefore, tungsten on HZSM-5 aided methane conversion and contributed to high coke selectivities.

In catalyst 1.8W3.0M/HZSM-5 where the amount of W was low and the amount of Mo was high, there was no selectivity towards xylene despite showing high selectivity towards C_2 hydrocarbons. In catalyst 3.0W1.8M/HZSM-5 where the amount of W was high and the amount of Mo was low, the resultant catalyst displayed moderate activity in methane conversion, least selectivity towards C_2 hydrocarbons but most selectivity towards benzene.

When Mo/HZSM-5 catalyst is used alone, methane hydrogenates and dimerizes on Mo species (Solymosi *et al.*, 1999). Various reports on bifunctional catalysis of Mo/HZSM-5 (Wang *et al.*, 1993) have shown that MoO_3 crystallites are the active sites for methane activation. The active component of the catalyst arises from the interaction between MoO_3 and the acid sites of the HZSM-5 zeolite (Zhang *et al.*, 1998). During calcination, the MoO_3 species diffuses into the HZSM-5 where it interacts with the Bronsted acid sites. Once inside the zeolite channel, the MoO_3 reacts with H^+ associated with Bronsted acid sites to form $[MoO_2(OH)]^+$ species, which condenses to form $[MoO_2(H_2O)]$ dimers and H_2O.

In NOCM reaction, a methane molecule is activated on the catalyst surface to form CH_3^* radicals which undergo further transformation into aromatics. The reaction mechanism encompasses catalysis for the formation of C_2H_6 by metal oxide species. During this stage, metal oxide species reacts with methane to yield a specific carbonaceous intermediate on the catalyst surface, which is further transformed into C_2H_6 by continuous reactions of methane with the CH_3^* radicals. Further, methane reacts with metal ions on HZSM-5 to produce CH_3^+ (a methoxy species on the Bronsted acid sites of the zeolite) which are further converted into a metal-carbene species, (Metal=CH_2). The formed methyl radicals (CH_3^*) are coupled to produce C_2H_6 which is further transformed into benzene through oligomerization and cyclization reactions. In typical W-Mo/HZSM-5 catalyst system, synergetic effect of noble metals comes into play in conversion of methane to carbon and petrochemicals where W was desired for methane conversion and coke selectivity. On the other hand, molybdenum was desired for generation of methyl radicals which were oligomerized into C_2H_6. Bronsted acid sites and shape selectivity of HZSM-5

was provided an avenue for conversion C_2 intermediates into benzene and its derivatives.

Table 3
Methane Conversion and Product Selectivity of Various Catalysts Loaded on HZSM-5 at 750℃, and GHSV 0.96 $Lg^{-1}cat.h^{-1}$

No.	Catalyst	Methane Conversion (%)	C_2 selectivity (%)	Aromatic selectivity			Coke selectivity (%)
				Benzene (%)	Toluene (%)	Xylene (%)	
1.	4.8M/HZSM-5	3.89	12.31	47.72	11.93	0.00	40.35
2.	4.8W/HZSM-5	15.19	8.48	44.78	9.80	0.00	45.42
3.	2.4W2.4M/HZSM-5	11.34	6.22	63.14	10.14	0.46	26.42
4.	1.8W3.0M/HZSM-5	6.92	13.29	51.70	6.07	0.00	42.23
5.	3.0W1.8M/HZSM-5	12.54	2.90	64.42	8.32	0.22	27.04

2.4.3. *Characterization of Spent Catalyst*

2.4.3.1. *TEM Analysis of Deposited Carbon*

From Fig. 4 below, TEM images of deposited carbon nanomaterial are seen on each catalyst. Carbon nanotubes (CTs) and nanoparticles of metal oxides are seen in the catalyst 4.8M/HZSM-5. From the TEM micrographs of catalyst 4.8W/HZSM-5, a dense mass of carbon nanomaterial is seen deposited on the spent catalyst. This implies that the carbon nanotubes formed on 4.8M/HZSM-5 catalyst was largely due to the presence of Mo. Few uniform CNTs with smooth external surfaces and metal oxide nanomaterial are formed on catalyst 2.4W2.4W/HZSM-5. Despite the presence of Mo which is believed to have yielded carbon nanotubes in catalyst 2.4W2.4M/HZSM-5), no significant amount of carbon nanotubes were formed on catalyst. This implies that tungsten promoted Mo dispersion into the zeolite. In catalyst 1.8W3.0M/HZSM-5, a dense mass of irregular shaped carbon nanomaterial was formed. In catalyst 3.0W1.8M/HZSM-5, neat structures of carbon nano material were formed on the catalyst. We can therefore speculate that low yields of carbon nanotubes with low index planes in all catalysts other than 4.8M/HZSN-M-5) were due to high dispersion of metal oxides in the zeolite which were unable to effectively activate the C-H bond in methane (Li *et al.*, 2016). Molybdenum is known to promote the growth of carbon nanotubes but since its metal loading in catalyst 3.0W1.8M/HZSM-5) is too low, its ability to promote the growth of carbon nanotubes is impaired because it is completely dispersed in the zeolite (Bajec *et al.*, 2019).

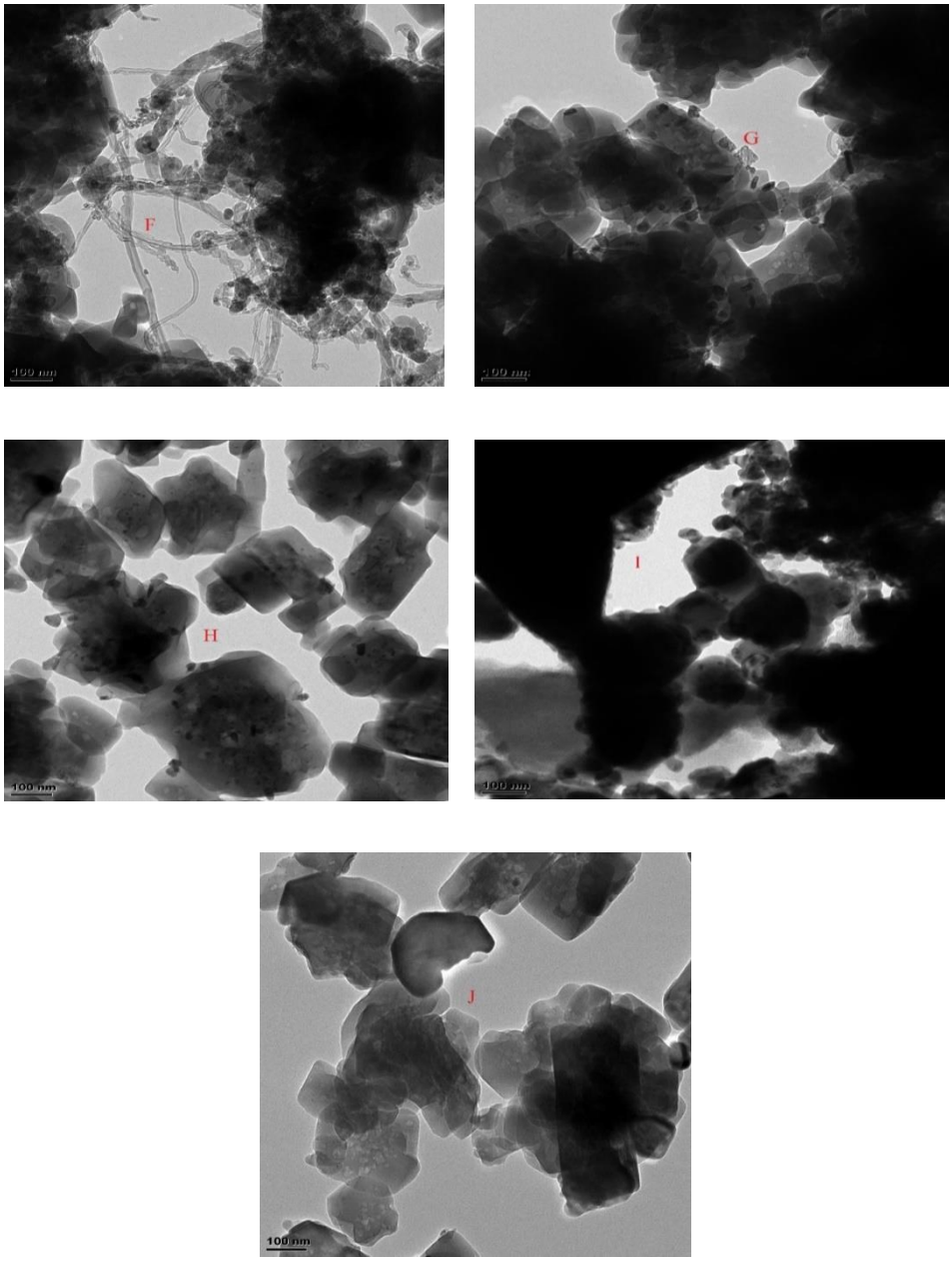

Fig. 4 – TEM Image of catalysts; F(4.8M/HZSM-5), G(4.8W/HZSM-5), H(2.4W2.4M/HZSM-5), I(1.8W3.0M/HZSM-5), and J(3.0W1.8M/HZSM-5).

3. Conclusions

This present work demonstrates the development of a stable and durable W-Mo/HZSM-5 catalyst system for methane conversion and quantitative determination of product distribution in non-oxidative conversion of methane into carbon and petrochemicals. Based on the results obtained, metal loading and synergism in the catalyst system played a significant role on methane conversion and product distribution. In a nutshell, a catalyst system with 4.8%Mo supported on HZSM-5 zeolite was less active in methane conversion but most selective towards toluene. A catalyst system with 4.8%W supported HZSM-5 was most active in methane conversion, less selective towards benzene, and most selective towards coke. A combination of 2.4%W and 2.4%Mo on HZSM-5, was less active on methane conversion compared to catalyst 4.8W/HZSM-5 but displayed good results in terms of selectivity towards benzene, least selective towards coke, and most selective towards xylene. In catalyst 1.8W3.0M/HZSM-5 where the amount of W was low and the amount of Mo was high, there was no selectivity towards xylene despite showing high selectivity towards C_2 hydrocarbons. In catalyst 3.0W1.8M/HZSM-5 where the amount of W was high and the amount of Mo was low, there was moderate activity in methane conversion, least selectivity towards C_2 hydrocarbons but most selective towards benzene. Therefore, in the binary W-Mo/HZSM-5 catalyst system, tungsten aided methane conversion and promoted coke selectivity while molybdenum aided generation of methyl radicals which were oligomerized into C_2 hydrocarbons. The channel structure, Bronsted acid sites, thermal stability, and shape selectivity of HZSM-5 provided an avenue for conversion C_2 intermediates into benzene and its derivatives.

The development of a binary W-Mo/HZSM-5 catalyst system catalyst system which is catalytically active in non-oxidative methane conversion and selective towards useful fuels and petrochemicals with over 10% methane conversion up to 4 h time on stream has been demonstrated. It has also been demonstrated that by varying the amount of W and Mo in the catalyst systems when supported on HZSM-5, such a catalyst system can be tuned to achieve optimum methane conversion and selectivity towards useful petrochemicals.

Acknowledgements. We sincerely thank Durban University of Technology for allowing us to use its laboratory and library in conducting this research.

REFERENCES

Abdelsayed V., Shekhawat D., Smith M.W., *Effect of Fe and Zn Promoters on Mo/HZSM-5 Catalyst for Methane Dehydroaromatization*, Fuel, **139**, 401-410 (2015).

Ali M.A., Tatsumi T., Masuda T., *Development of Heavy Oil Hydrocracking Catalysts Using Amorphous Silica-Alumina and Zeolites as Catalyst Supports*, Applied Catalysis A: General, **233**, *1*, 77-90 (2002).

Bajec D., Kostyniuk A., Pohar A., Likozar B., *Nonoxidative Methane Activation, Coupling, and Conversion to Ethane, Ethylene, and Hydrogen over Fe/HZSM-5, Mo/HZSM-5, and Fe-Mo/HZSM-5 Catalysts in Packed Bed Reactor*, International Journal of Energy Research, **43**, *13*, 6852-6868 (2019).

Brandt A.R., Masnadi M.S., Englander J.G., Koomey J., Gordon D., *Climate-Wise Choices in a World of Oil Abundance*, Environmental Research Letters, **13**, 4, 044027 (2018).

Burns S., Hargreaves J.S.J., Pal P., Parida K.M., Parija S., *The Effect of Dopants on the Activity of MoO3/ZSM-5 Catalysts for the dehydroaromatisation of Methane*, Catalysis Today, **114**, *4*, 383-387 (2006).

Campbell S.M., Bibby D.M., Coddington J.M., Howe R.F., Meinhold R.H., *Dealumination of HZSM-5 Zeolites: I. Calcination and Hydrothermal Treatment*, Journal of Catalysis, **161**, *1*, 338-349 (1996).

Chen B., Li J., Wu X., Han M., Zeng L., Li Z., Chen G., *Global Energy Flows Embodied in International Trade: A Combination of Environmentally Extended Input–Output Analysis and Complex Network Analysis*, Applied Energy, **210**, 98-107 (2018).

Cheng X., Yan P., Zhang X., Yang F., Dai C., Li D., Ma X.-X., *Enhanced Methane Dehydroaromatization in the Presence of CO_2 over Fe-and Mg-Modified Mo/ZSM-5*, Molecular Catalysis, **437**, 114-120 (2017).

Ding W., Meitzner G.D., Iglesia E., *The Effects of Silanation of External Acid Sites on the Structure and Catalytic Behavior of Mo/H–ZSM5*, Journal of Catalysis, **206**, *1*, 14-22 (2002).

Fujikawa T., Idei K., Ebihara T., Mizuguchi H., Usui K., *Aromatic Hydrogenation of Distillates over SiO_2-Al_2O_3-Supported Noble Metal Catalysts*, Applied Catalysis A: General, **192**, *2*, 253-261 (2000).

Karakaya C., Kee R.J., *Progress in the Direct Catalytic Conversion of Methane to Fuels and Chemicals*, Progress in Energy and Combustion Science, **55**, 60-97 (2016).

Karakaya C., Zhu H., Loebick C., Weissman J.G., Kee R.J., *A Detailed Reaction Mechanism for Oxidative Coupling of Methane over Mn/Na2WO4/SiO2 Catalyst for Non-Isothermal Conditions*, Catalysis Today, **312**, 10-22 (2018)

Khan T.S., Balyan S., Mishra S., Pant K.K., Haider M.A., *Mechanistic Insights into the Activity of Mo-Carbide Clusters for Methane Dehydrogenation and Carbon-Carbon Coupling Reactions to Form Ethylene in Methane Dehydroaromatization*, Phys. Chem. C, **122**, 22, 11754-11764 (2018).

Li J., Dong L., Xiong L., Yang Y., Du Y., Zhao L., Wang H., Peng S., *High-Loaded $NiCuSiO_2$ Catalysts for Methane Decomposition to Prepare Hydrogen and Carbon Filaments*, International Journal of Hydrogen Energy, **41**, *28*, 12038-12048 (2016).

Liu C.-J., Yu K., Zhang Y.-P., Zhu X., He F., Eliasson B., *Characterization of Plasma Treated Pd/HZSM-5 Catalyst for Methane Combustion*, Applied Catalysis B: Environmental, **47**, *2*, 95-100 (2004).

Liu H., Wu S., Guo Y., Shang F., Yu X., Ma Y., Xu C., Guan J., Kan Q., *Synthesis of Mo/IM-5 Catalyst and its Catalytic Behavior in Methane Non-Oxidative Aromatization*, Fuel, **90**, *4*, 1515-1521 (2011).

Liu S., Wang L., Ohnishi R., Ichikawa M., *Bifunctional Catalysis of Mo/HZSM-5 in the Dehydroaromatization of Methane to Benzene and Naphthalene XAFS/TG/DTA/MASS/FTIR Characterization and Supporting Effects*, Journal of Catalysis, **181**, *2*, 175-188 (1999).

Liu Z., Li L., Iglesia E., *Catalytic Pyrolysis of Methane on Mo/H-ZSM5 with Continuous Hydrogen Removal by Permeation through Dense Oxide Films*, Catalysis Letters, **82**, *3-4*, 175-180 (2002).

Ma S., Guo X., Zhao L., Scott S., Bao X., *Recent Progress in Methane Dehydroaromatization: From Laboratory Curiosities to Promising Technology*, Journal of Energy Chemistry, **22**, *1*, 1-20 (2013).

Ohnishi R., Liu S., Dong Q., Wang L., Ichikawa M., *Catalytic Dehydrocondensation of Methane with CO and CO_2 Toward Benzene and Naphthalene on Mo/HZSM-5 and Fe/Co-Modified Mo/HZSM-5*, Journal of Catalysis, **182**, *1*, 92-103 (1999).

Rodrigues A.C.C., Monteiro J.L.F., *The Use of CH_4/H_2 Cycles on Dehydroaromatization of Methane over MoMCM-22*, Catalysis Communications, **9**, *6*, 1060-1065 (2008).

Sily P.D., Noronha F.B., Passos F.B., *Methane Direct Conversion on Mo/ZSM-5 Catalysts Modified by Pd and Ru*, Journal of Natural Gas Chemistry, **15**, *2*, 82-86 (2006).

Solymosi F., Bugyi L., Oszko A., Horvath I., *Generation and Reactions of CH_2 and C_2H_5 Species on Mo_2C/Mo (111) Surface*, Journal of Catalysis, **185**, *1*, 160-169 (1999).

Solymosi F., Szöke A., Cserenyi J., *Conversion of Methane to Benzene over Mo_2C and Mo_2C/ZSM-5 Catalysts*, Catalysis Letters, **39**, *3-4*, 157-161 (1996).

Tan P., Leung Y., Lai S., Au C., *The Effect of Calcination Temperature on the Catalytic Performance of 2 wt.% Mo/HZSM-5 in Methane Aromatization*, Applied Catalysis A: General, **228**, *1-2*, 115-125 (2002).

Varghese J.J., Saravanan B., Vach H., Peslherbe G.H., Mushrif S.H., *First-Principles Investigation of the Coupling-Induced Dissociation of Methane and its Transformation to Ethane and Ethylene*. Chemical Physics Letters, Elsevier, ffhal-02401222 (2018).

Wang D., Lunsford J.H., Rosynek M.P., *Catalytic Conversion of Methane to Benzene over Mo/ZSM-5*, Topics in Catalysis, **3**, *3-4*, 289-297 (1996).

Wang D., Lunsford J.H., Rosynek M.P., *Characterization of a Mo/ZSM-5 Catalyst for the Conversion of Methane to Benzene*, Journal of Catalysis, **169**, *1*, 347-358 (1997).

Wang L., Tao L., Xie M., Xu G., Huang J., Xu Y., *Dehydrogenation and Aromatization of Methane under Non-Oxidizing Conditions*, Catalysis Letters, **21**, *1-2*, 35-41 (1993).

Wassie S.A., Cloete S., Spallina V., Gallucci F., Amini S., van Sint Annaland M., *Techno-Economic Assessment of Membrane-Assisted Gas Switching Reforming for Pure H_2 Production with CO_2 Capture*, International Journal of Greenhouse Gas Control, **72**, 163-174 (2018).

Wu P., Kan Q., Wang X., Wang D., Xing H., Yang P., Wu T., *Acidity and Catalytic Properties for Methane Conversion of Mo/HZSM-5 Catalyst Modified by Reacting with Organometallic Complex*, Applied Catalysis A: General, **282**, 1-2, 39-44 (2005).

Xu Y., Lin L., *Recent Advances in Methane Dehydro-Aromatization over Transition Metal Ion-Modified Zeolite Catalysts under Non-Oxidative Conditions*, Applied Catalysis A: General, **188**, *1-2*, 53-67 (1999).

Xu Y., Liu S., Guo X., Wang L., Xie M., M*ethane Activation without Using Oxidants over Mo/HZSM-5 Zeolite Catalysts*, Catalysis Letters, **30**, *1-4*, 135-149 (1994).

Xu Y., Wang J., Suzuki Y., Zhang Z.-G., *Effect of Transition Metal Additives on the Catalytic Stability of Mo/HZSM-5 in the Methane Dehydroaromatization under Periodic CH4–H2 Switch Operation at 1073K*, Applied Catalysis A: General, **409-410**, 181-193 (2011).

Xu Y., Wang J., Suzuki Y., Zhang Z.-G., *Improving Effect of Fe Additive on the Catalytic Stability of Mo/HZSM-5 in the Methane Dehydroaromatization*. Catalysis Today, **185**, *1*, 41-46 (2012).

Zeng J.L., Xiong Z.T., Zhang H.B., Lin G.D., Tsai K., *Nonoxidative Dehydrogenation and Aromatization of Methane over W/HZSM‐5‐Based Catalysts*, Catalysis Letters, **53**, *1-2*, 119-124 (1998).

Zhang C.-L., Li S., Yuan Y., Zhang W.-X., Wu T.-H., Lin L.-W., *Aromatization of Methane in the Absence of Oxygen over Mo-Based Catalysts Supported on Different Types of Zeolites*, Catalysis Letters, **56**, *4*, 207-213 (1998).

INFLUENȚA CONCENTRAȚIEI ȘI SINERGIA COMPONENȚILOR METALICI ASUPRA CATALIZATORULUI BINAR W-MO / HZSM-5 PENTRU CONVERSIA NEOXIDATIVĂ A METANULUI ÎN CARBON ȘI PRODUSE PETROCHIMICE

(Rezumat)

Prelucrarea energiei din combustibili fosili este asociată cu emisia de compuși carbonici. Prin urmare, conversia neoxidativă a metanului în carbon și produse petrochimice remediază emisia acestor gaze cu efect de seră în atmosferă. Prezentul studiu demonstrează dezvoltarea unor sisteme de catalizator binar stabile, durabile și reglabile, care cuprind W, și Mo depuse pe HZSM-5. Sistemele de catalizator au fost sintetizate prin impregnare umedă, caracterizate și testate pentru conversia neoxidativă a metanului într-un reactor cu strat fix. Efluenții reactorului au fost analizați folosind cromatografia gazoasă. Pe baza rezultatelor obținute, reacțiile concurente între diferite specii de metal, încărcarea și sinergismul au influențat distribuția produsului. Molibdenul carburat (M2C) pe zeolitul HZSM-5 singur a prezentat o activitate catalitică redusă, dar la introducerea W ca promotor de reacție, activitatea sa a crescut enorm. Reacția a presupus disocierea moleculelor de metan pe Mo carburat pentru a forma specii C_2 ca intermediari primari care au fost oligomerizați în continuare în compuși aromatici și hidrocarburi superioare în canalele zeolitului HZSM-5.